Lawrence Berkeley National Laboratory

Title

Bimolecular crystal instability and morphology of bulk heterojunction blends in organic and perovskite solar cells

Permalink

https://escholarship.org/uc/item/439061wv

Authors

Song, Jingnan
Hu, Qin
Zhang, Ming
et al.

Bimolecular Crystal Instability and Morphology of Bulk heterojunction Blends in Organic and Perovskite Solar Cells

Jingnan Song[1†], Qin Hu[2,3†], Ming Zhang[1], Zengquan Zhang[1], Lei Zhu[1], Jazib Ali[1], Jinqiu Xu[1], Cheng Wang[4], Rui Zhu[*5,6,7], Feng Liu[*1] and Thomas Russell[*2,3],

[1]School of Physics and Astronomy, Shanghai Jiao Tong University, 200240, Shang Hai, China

[2]Department of Polymer Science and Engineering, University of Massachusetts, Amherst, MA 01003, USA

[3]Materials Sciences Division, Lawrence Berkeley National Laboratory, CA, 94720, USA

[4]Advanced Light Sources, Lawrence Berkeley National Laboratory, CA, 94720, USA

[5]State Key Laboratory for Artificial Microstructure and Mesoscopic Physics, School of Physics, Peking University, Beijing, 100871, China

[6]Collaborative Innovation Center of Quantum Matter, Beijing, 100871, China

[7]Collaborative Innovation Center of Extreme Optics, Shanxi University, Taiyuan, Shanxi, 030006, China

[†]Jingnan Song and Qin Hu contributed to this work equally.
[*]Address correspondence to: fengliu82@sjtu.edu.cn, iamzhurui@pku.edu.cn, tom.p.russell@gmail.com

Abstract

The performance of polymer:fullerene bulk heterojunction (BHJ) solar cells is significantly influenced by the morphology of the electron donor and acceptor blend under the premise that electronic structure is complimentary in absorption regarding to donor and acceptor materials. There are many cases where intimate mixing of the donor and acceptor perturbs the electronic structure, which fundamentally changes the transport and photovoltaic characteristics. Here, we present the bimolecular crystal packing of polymers and fullerenes and investigated the correlation between device function and structural details. We find that bimolecular crystallization can reorganize polymer chain packing, leading to poor electron transport and solar cell performance. The size compatibility and the mitigation of the entropy penalty led to a co-crystallization instability, which as evidenced by *in situ* x-ray diffraction. PCBM is found to intercalate between the side chains of PQT by a reorganization of both PQT and PCBM, forming stable, highly ordered bimolecular crystals The poor electron transport in the bimolecular crystal domain accounts for the poor device performance in both perovskite and organic solar cells. BisPCBM, on the other hand, only forms loosely packed aggregates in solution, that rapidly phase separate into large domains with an edge-on interfacial orientation and performed poorly in solar cells.

1. Introduction

Blending an organic semiconducting donor with an acceptor, in general, leads to a phase separated bulk heterojunction (BHJ) morphology that, due to an increase in

interfacial area and independent electron and hole transport domains, is favorable for photovoltaic applications, yielding reported power conversion efficiencies of up to ~15% in single layered solar cells.[1-3] The transport and performance of BHJ solar cells is heavily influenced by the nanoscopic structure of the donor/acceptor blends, where domain size and purity, ordering and orientation of components within the domains and at the interfaces with the electrodes, and the characteristics of the interface between the domains dictate exciton dissociation, recombination and charge transport.[4-6] In general, a bicontinous morphology with domains tens of nanometers in size, where the domains are either pure donor or acepotor, is desirable to balance exciton splitting and carrier hopping. Partial mixing of the donor and acceptor is generally considered to be detrimental to the performance, though there are cases where the donor and acceptor form guest-host bimolecular crystals, that can enhance performance, but manipulation and optimization of the morphology is challenging.[7-10] One case in point are mixtures of PBTTT (poly(2,5-bis(3-tetradecyllthiophen-2-yl)thieno[3,2-b]thiophene)) and $PC_{70}BM$ (phenyl-c71-butyric acid methyl ester) where the PBTTT side chain can host $PC_{70}BM$, suppress π-π stacking of the polymer chains, forming bimolecular crystals at the eutectic temperature.[5, 11] Guest-host size and temperature are determining factors that guide the bimolecular crystallization, which in-turn, affect the performance of photovoltaic devices.[5, 12, 13]

Revealing the structure and morphology of the blends at all length scales and at interfaces, and relating these to the transport and photovoltaic properties, is of general interest for gaining insights into organic semiconducting materials. PQT (Poly(3, 3'-

didodecylquaterthiophene)) is a well-established hole-transporting semi-crystalline polymer that has large side-chain vacancies to accommodate guest molecules. Highly ordered crystalline packing can be produced by side-chain interdigitation.[14-16] However, this is not a good photovoltaic material, showing a low power conversion efficiency (PCE) of only ~0.4%.[17, 18] Whether the poor performance is a result of the intrinsic properties of PQT or the morphology is an open question. To address this, we performed morphological studies on the bimolecular crystallization PQT of mono- and bis-fullerene adducts using scattering and imaging methods and correlated this to their performance in organic solar cells. The miscibility of PQT with the mono- and bis-fullerene adducts was found to be different, leading to distinctly different phase separation behavior and interfacial orientation. Size compatibility was found to be a major factor in governing the bimolecular intercalation in thin film blends. In wet films, the bis-fullerene adduct can form an ordered bimolecular structure, that rearranged as the solvent evaporated. The bimolecular crystals are not efficient electron transporters, requiring excessive amounts of PCBM to function.

Results and Discussions

Fig. 1a-b shows the chemical structures of PQT, PCBM, and BisPCBM, as well as the UV-vis absorption spectra. The polythiophene backbone and regularly spaced dodecyl side chains make it a good host for fullerene molecules. In neat thin films, a semi-crystalline π-π stacked lamellar morphology forms good transport channels; partial interdigitation of the side-chains from adjacent lamellae occurs in PQT, promoting three dimensional order.[14] Absorption spectra of pure PQT, PQT:Fullerene

(PCBM and BisPCBM) blends with different weight ratios are shown in Fig. 1b. Here, the 1:1 and 1:4 weight ratios of PQT and PCBM are abbreviated as PQT-M1 and PQT-M2, and the 1:1 and 1:4 weight ratios of PQT and BisPCBM are abbreviated as PQT-M3 and PQT-M4. The pure PQT film exhibits a strong absorption in the range from 400 to 625 nm, with a well-resolved resonant shoulder at ~600 nm, attributed to the ordering of PQT chains. When PQT is blended with PCBM, the resonance is disrupted, indicating a fundamental change in electronic structure. The 600 nm shoulder in the PQT-M2 blends disappears, so the π-π stacking of PQT is also disrupted. This is similar to the results found for PBTTT:PCBM blends.[8] PQT:PCBM blends show a similar absorption as PQT in neat films with good resonance structures. Therefore, PQT-PQT contacts are maintained.

Grazing incidence wide-angle x-ray scattering (GIWAXS) was used to study the molecular packing and crystallization of PQT:PCBM blend. As shwon in Fig. 1c and Fig. S1 (black curve), PQT crystallizes, with the (100) peak at 0.32 $Å^{-1}$ (with crystal coherence length (CCL) of 13.9 nm), the (001) peak at 0.49 $Å^{-1}$ (with a CCL of 15.7 nm), and the (010) peak at 1.60 $Å^{-1}$ (with a CCL of 10.5 nm) evident in the data. Blending PQT with BisPCBM lead to less ordered PQT packing, as evidenced by the sharp decrease these signature peaks of PQT, but the development of a new structure is not evident. PQT:PCBM blends showed quite different behavior. As seen in PQT-M1 thin films, a sharp reflection is seen at 0.197 $Å^{-1}$ (with a CCL of 19.6 nm), indicating and increase in the lamellae spacing, suggesting the incorporation of PCBM into the PQT forming bimolecular crystals, decreasing the interdigitation and forcing

the PQT chains apart. It should be noted that two new peaks appeared 0.66 Å^{-1} (with a CCL of 17.9 nm) and 1.75 Å^{-1} (with a CCL of 9.4 nm). The PQT π-π stacking distance is ~3.9 Å and fullerene has a diameter of 7 Å. This suggests that 2-3 PQT layers could host one PCBM. The 0.66 Å^{-1} reflection is assigned to PCBM separation distance and the 1.75 Å^{-1} peak is assigned to a reorganized π-π stacking distance. Such a well-organized structure with better PCBM ordering in the solid state would be expected to have good electron transport, but that is not the case. Fig. 1d and Fig. S2 show the bilayer thin films (PQT was transfer printed onto PCBM layers) at different thermal annealing temperatures for 15 min. Such a treatment should reveal details on the diffusion of PCBM into PQT. PQT:PCBM bilayers annealed at 85 °C showed a quite complicated structure, with a sharp primary reflection at 0.20 Å^{-1}, which we attribute to a PCBM diffusion-induced bimolecular crystal formation, with even tighter packing than that seen in the BHJ thin film. Thermal annealing at 150 °C produced a primary peak at 0.23 Å^{-1}, which is similar to the solution preparation. These results indicate that PQT:PCBM bimolecular crystals are a thermally stable species. PQT:BisPCBM bilayer experiments showed similar results as in solution prepared BHJ thin film. Consequently, BisPCBM can only diffuse into PQT amorphous regions with thermal annealing.

In situ GIWAXS was used to measure the time evolution of the morphology of PQT:fullerene blends from the solution to the final film on drop-cast thin films, as shown in Fig. 2 and Fig. S3. The diffuse reflection at q~1.8 Å^{-1} is attributed to the solvent and was used to assess the solvent evaporation from the film. As seen in the

scattering profiles, a rapid decrease in the scattering occurs at frame 9 and vanishes by frame 13, indicating the conversion from a solution to a solid film. At frame 5, prior to the removal of all the solvent, the (100) reflection, characteristic of the bimolecular crystal is evident.   As solvent evaporates (from frame 10 to 15), the distance corresponding to the (100) **reflection decreases from _____ to _____,** indicating that when the solvent solubilizes the side chains, inter-chain separation distance ioncreases. **Thus, such state is even stable under solution condition, indicating a high entropy gain in its formation.** In the early state bimolecular crystal formation the interplane distance is slightly larger, due to the incorporation of solvent molecules.LiquidThe solution to solid-state transition leads to a reorganization of the bimolecular crystal, as evidenced by the interplane distance decrease. A schematic presentation of this such process is shown in Fig. 2d. The *in situ* PQT:BisPCBM experiment showed a more complicated behavior. The liquid to solid-state transition occurred from frames 14 to 19. PQT in solution state can form some interdigitated (100) packing, as seen from a low inter-plane distance (~22 Å) at frame 5. This value then increased to ~27 Å at frame 10, indicating the formation of the BisPCBM bimolecular crystals. This crystal is not stable, and rapidly changed to a PQT crystalline packing. PQT and bimolecular crystals form before the solidification, the low q region can be split into two peaks, as seen from the hexagon and square symbols in the   plots (Fig. 2c). When the film solidified (~frame 20), PQT:BisPCBM bimolecular crystals rapidly decomposed, a strong PQT crystallization drive trace solvent out, and the side chain packing changed and finally stabilized at ~21 Å. Such

in situ experiments showed quite intriguing results regarding the bimolecular crystallization of different pairs. The PQT:PCBM guest-host crystallization is stable, can undergo thermal annealing, and solvent etching; PQT:BisPCBM can only form bimolecular crystals in the presence of solvent with PQT loosely packed, which then rapidly changes to the more favorable PQT crystal. This difference can be traced from their packing nature. In PQT:PCBM blends, a strong bimolecular (100) packing, good PQT (010) packing, and good PCBM (100) packing were found. Thus, PQT:PCBM bimolecular crystal is a simple fusion of PQT and PCBM crystals, which form a lamellae structure through favorable electronic interactions. The PQT:BisPCBM bimolecular crystal is less favorable, due to the incompatibility of the PQT side chain and BisPCBM. BisPCBM with the two tails does not cocrystallize. Only in the presence of solvent, during when the PQT side chains are solubilized is BisPCBM found between the PQT lamellae. As the solvent evaporates during the liquid to solid transition, BisPCBM is forced out from between the PQT chains. The schematic for this process is shown in Fig. 2e.

Phase separation, including length scale and purity of the domains, in the BHJ active layer will significantly impact device performance. Fig. 3 shows the transition electron microscopy (TEM), resonant soft X-ray scattering (RSoXS), and grazing incident small angle X-ray scattering (GISAXS) data, used to probe the morphology of th active layer. As shown in Fig. 3a, the PQT:PCBM blends at a weight ratio of 1:1 and 1:4 show a uniform morphology with small sized omains. The PQT:BisPCBM 1:1 blends shows phase separation on a much larger length scale ~100 nm. The

PQT:BisPCBM 1:4 blend shows larger domains, consisting of BisPCBM aggregates. RSoXS experiment was performed (Fig. 3b) at a photon energy of 284.2 eV. PQT:PCBM 1:1 blends showed an interference at 0.015 Å^{-1}, corresponding to a distance of 42 nm. Any interferences arising from a phase separated morphology for the PQT:PCBM 1:4 blend were much less pronounced. The PQT:BisPCBM blends, on the other hand, showed quite strong interferences at at 0.006 Å^{-1} (distance of 105 nm) for the1:1 blend and at 0.005 Å^{-1} (distance of 125 nm) for the 1:4 blend. Fig. 3c shows the GISAXS profiles of PQT:fullerenes blends that covers larger q range. Quit similar results were obtained by GISAXS.

With RSoXS, the polarization of the incident x-rays can also be used to probe the orientation of specific dipoles at the interface between domains and, hence, chain orientation induced by the presence of an interface.[22] Using the PQT-M4 system as an example, Fig. 4a shows that the photon energy and electric field direction of the X-rays give rise to markeldy different scattering profiles from which a dichroism, σ, reflecting segmental orientation can be determined by $\sigma = \dfrac{(I_{90} - I_{180})}{(I_{90} + I_{180})}$., as shown in Fig. S4. [23, 24] With s polarization, the scattering intensity in the vertical direction was significantly enhanced at 285.0 eV (σ=0.17), the polymer 1s-π* transition. At a photon energy of 287.3 eV, the polymer 1s-$\sigma*¿$ transition, polarization factor changed to -0.29. These results suggest an edge-on orientation of PQT at the interface of the domains. For an x-ray energy far below or above the absorption edge of polymer (285 eV), the scattering profiles are more isotropic. By changing the polarization of the x-rays from

s- to p-polarization, the lobes in the scattering rotated from being centered at 90° to being centered at 0° (180°), as shonw in Figure 4B. Neither the location of the masimum in th scattering nor the azimuthal spread of the data changed with the polarization rotation. This indicates that the domains are, on average, isotropic, and the scattering reflects the orientation of the PQT segments at the domains boundaries, as seen in other systems. .

To investigate the relationship between molecular packing and device performance, the solution-processed BHJ organic solar cells were fabricated with the PQT as the electron donor and PCBM or BisPCBM as the electron acceptor using a conventional device architecture of indium-tin oxide (ITO)/poly (3,4-ethylenedioxythiophene):poly(styrenesulfonate) (PEDOT:PSS)/BHJ blends/Al (Fig. 5a). Fig. 5b show the light current-voltage (J-V) curves of the devices with PQT:fullerene as the active layer. Details of the device parameters (J_{sc}, V_{oc}, FF, and PCE) are provided in Table S1. A strong dependence of the device performance on the PQT:fullerene weight ratios and electron acceptors. PQT:PCBM 1:1 blends showed a inferior device performance with a low Voc of 0.46 eV, which is well below that from polythiophene based donor polymers. A large fraction of PQT would be incorporated into the bimolecular crystals, leaving amorphous PQT to mix with PCBM forming a low-density acceptor domain. Such a morphology, though, is not ideal electronically to generate carriers. Bimolecular crystal with a high amount of PCBM loading could give rise to quenching, and electron transport in the mixed region would also be poor. These contribute to a low FF and small Jsc. For PQT:PCBM 1:4 blends, the best

device showed a PCE of 0.96%, which is four times that of 1:1 blended thin film. A Voc of 0.74 V was recorded, which is well above polythiophne:PCBM blends. The power output voltage increase indicates a fundamental change in electronic structure that constitutes the BHJ functioning domains. High PCBM loading makes the electron transport quite efficient, and it is expected that the bimolecular crystal in this condition could be the electron donor, deepening the hybrid new LUMO, leading to a Voc increase. PQT:BisPCBM 1:1 blends showed a Voc of 0.66 V and a Jsc of 2.28mA/cm^2, which is in normal for this mixture. Adding more BisPCBM led to drop in the Voc and Jsc, opposite to that for the PQT:PCBM blends. For the PQT: BisPCBM blend, as evidenced by the strong scattering, a very well-defined phase separated morphology forms and the decrease in Voc is expected by the change in the electronic structure of the mixed, amorphous PQT:BisPCBM domains.

To investigate the effects of molecular packing on the electron transport properties, perovskite solar cells with different PQT:PCBM weight ratios as an electron transporting layer (ETL) were fabricated. The device structure of perovskite solar cells is shown in Fig. 5a. The PTAA was deposited on ITO glass substrate as a hole transporting layer. MAPbI$_3$ was spin-coated using antisolvent methods.[25, 26] Then, PQT:PCBM ETL was spin coated onto the perovskite film. Fig. **5c** shows the J-V curves of perovskite solar cells with different weight ratios of PQT:PCBM as the electron transporting layer, and the corresponding device parameters are given in Table S2. Detailed performance parameters (PCE, J_{SC}, V_{OC}, and FF) are shown in Fig. S5. It is clear that the concentration of of PQT significantly affects device performance.

PQT:PCBM 1:1 blends had a very low Voc and Jsc, a much poorer performance than that when P3HT:PCBM blends were used as the electron transporting layers. Consequently, we can conclude that the bimolecular crystal is not a good electron transporting media. By increasing the PCBM loading. the 1:2 blends showed a significantly improved Jsc, Voc and FF, indicating that $PC_{60}BM$ forms a good electron transport pathway. Increasing the weight ratio to 1:8, a higher efficiency was achieved, with a champion efficiency of 16.68% (Fig. 5d), which is comparable to pure PCBM transporting layers. However, under such conditions a very large hysteresis was found, indicating that the bimolecular crystal can block and switch transport in perovskite solar cells.

2. Conclusions

In summary, this work demonstrates the kinetics of formation and instability of PQT:PCBM/BisPCBM bimolecular crystals and their performance in BHJ solar cells and as electron transporting layers. The PQT:BisPCBM bimolecular crystal is thermally-dynamic intrinsically unstable, existing only in the presence of solvent. Both the molecular packing and the length scale of phase separation in polymer/fullerene BHJ film have a significant effect on the device performance. For PQT:PCBM, the stable bimolecular crystal incorporates a large amount of PCBM, so a high PCBM concentration is necessary to achieve good electron transport, making the bimolecular domain function as an electron donor, so carriers generated from the bimolecular crystal domain can be extracted. For the PQT:BisPCBM blends, a bicontinous BHJ morphology forms, but the PQT crystalline order is poor. There is strong interfacial

orientation of PQT at the domain boundaery with the BisPCBM rich domains. leading to a decrease in device performance but a better FF. Good electron transport is obtained at a PQT:PCBM blend ratio of 1:8, which can be used in perovskite solar cells as an electron transport layer. Our work can provide guidance in the design of effective active layer materials and optimization of blend ratios for device optimization..

3. Experimental section

Materials: PQT was purchased from American Dye Source, Inc. Both PCBM and BisPCBM were ordered from Solenne, with the purity of 99.5%. PTAA and F4TCNQ were purchased from Xi'an Polymer Light Technology Corp. Lead iodide (98%) was purchased from TCI, and methylammoniumthe iodide (99.998%) was bought from Deysol. All the solvents were purchased from Acros.

Fabrication of bulk heterojunction organic solar cells: ITO glass (sheet resistance ≤ 10 Ω cm^{-2}) was cleaned consecutively in acetone, detergent, deionized water, and isopropanol ultrasonic bath for 15 min, respectively, and was dried at 70 $^{\circ}$C for 12 h. Then it was treated with UV-Ozone for 15 min before use. The PEDOT:PSS was spin-coated onto the ITO glass at 4000 rpm for 40 s, and baked in air at 150 $^{\circ}$C for 15 min. Then the substrate was transferred into glovebox for further device fabrication. The precursor solution of active layer (PQT:PCBM and PQT:BisPCBM) with different weight ratios was spin-coated at 1000 rpm for 30s onto the PEDOT:PSS layer. After deposition of the active layer, the sample was transferred into a vacuum chamber for further deposition of Al (100 nm) to finish the device fabrication process.

Fabrication of Perovskite solar cells: Firstly, the F4TCNQ doped PTAA with concentration of 2 mg/ml was spin coated on the UVO treated ITO glass at 5000 rpm for 30s, then thermal annealed at 150 ℃ for 10 min. Secondly, the perovskite precursor solution (MAI:PbI$_2$=1:1.08 was dissolved into the mixed DMF:DMSO solution, with volume ratio of 9:1) was spin coated on the ITO/PTAA film at 1000 rpm and 5000 rpm for 5s and 30s, respectively. During the last 23s of the second spin-coating step, the anti-solvent chlorobenzene was drop-casted，then 100 ℃ for 10 min. The PQT:PCBM with different weight ratios (15 mg/ml, 0:1, 1:1, 1:2, 1:4, 1:6, 1:8) was spin coated on the perovskite film at 2000 rpm for 30s. Finally, the 100 nm Al electrode was evaporated in a vacuum chamber.

Characterization: The GIWAXS and GISAXS measurements were conducted at beamline 7.3.3, Advanced Light Source (ALS), Lawrence Berkeley National Lab (LBNL). X-ray energy was 10 keV. RSoXS was performed at beamline 11.0.1.2 Lawrence Berkeley National Lab. Thin films was flowed and transferred onto Si3N4 substrate and experiment was done in transmission mode. Bright-field transmission electron microscopy (TEM) experiments were conducted with a JEOL 2000 FX TEM operating at an accelerating voltage of 200 kV. All the J-V curves in this study were recorded by using a Keithley 2400 source measurement unit under AM1.5G illumination with intensity of 100 mW cm^{-2}. The light intensity was calibrated with a standard Si photodiode detector.

Conflicts of interest

There are no conflicts to declare.

Acknowledge

References

1   S. Zhang, Y. Qin, J. Zhu and J. Hou, *Adv. Mater.,* 2018, **30**, e1800868.

2   H. Li, Z. Xiao, L. Ding and J. Wang, *Sci. Bulletin,* 2018, **63**, 340.

3   B. Kan, H. Feng, H. Yao, M. Chang, X. Wan, C. Li, J. Hou and Y. Chen, *Sci. China Chem.,* 2018, **61**, 1307.

4   Z. Zhou, S. Xu, J. Song, Y. Jin, Q. Yue, Y. Qian, F. Liu, F. Zhang and X. Zhu, *Nat. Energy,* 2018, **3**, 952.

5   A. C. Mayer, M. F. Toney, S. R. Scully, J. Rivnay, C. J. Brabec, M. Scharber, M. Koppe, M. Heeney, I. McCulloch and M. D. McGehee, *Adv. Func. Mater.,* 2009, **19**, 1173.

6   L. Nian, Y. Kan, H. Wang, K. Gao, B. Xu, Q. Rong, R. Wang, J. Wang, F. Liu, J. Chen, G. Zhou, T. P. Russell and A. K. Y. Jen, *Energy Environ. Sci.,* 2018, **11**, 3392.

7   N. C. Miller, E. Cho, M. J. Junk, R. Gysel, C. Risko, D. Kim, S. Sweetnam, C. E. Miller, L. J. Richter, R. J. Kline, M. Heeney, I. McCulloch, A. Amassian, D. Acevedo-Feliz, C. Knox, M. R. Hansen, D. Dudenko, B. F. Chmelka, M. F. Toney, J. L. Bredas and M. D. McGehee, *Adv. Mater.,* 2012, **24**, 6071.

8   J. E. Parmer, A. C. Mayer, B. E. Hardin, S. R. Scully, M. D. McGehee, M. Heeney and I. McCulloch, *Appl. Phys. Lett.,* 2008, **92**, 113309.

9   A. P. Yuen, J. S. Preston, A. -M. Hor, R. Klenkler, E. Q. B. Macabebe, E. Ernest van Dyk and R. O. Loutfy, *J. Appl. Phys.,* 2009, **105**, 016105.

10   B. C. Thompson, B. J. Kim, D. F. Kavulak, K. Sivula, C. Mauldin and J. M. J. Frechet, *Macromolecules,* 2007, **40**, 7425.

11   N. C. Miller, R. Gysel, C. E. Miller, E. Verploegen, Z. Beiley, M. Heeney, I. McCulloch, Z. Bao, M. F. Toney and M. D. McGehee, *J. Polym. Sci. Part B: Polym. Phys.,* 2011, **49**, 499.

12   N. C. Miller, S. Sweetnam, E. T. Hoke, R. Gysel, C. E. Miller, J. A. Bartelt, X. Xie, M. F. Toney, M. D. McGehee, *Nano Lett.* **2012**, 12, 1566.

13   P. Vemulamada, G. Hao, T. Kietzke and A. Sellinger, *Org. Electron.,* 2008, **9**,

661.

14   R. J. Kline, D. M. DeLongchamp, D. A. Fischer, E. K. Lin, L. J. Richter, M. L. Chabinyc, M. F. Toney, M. Heeney and I. McCulloch, *Macromolecules,* 2007, **40**, 7960.

15   E. Cho, C. Risko, D. Kim, R. Gysel, N. C. Miller, D. W. Breiby, M. D. McGehee, M. F. Toney, R. J. Kline and J. L. Bredas, *J. Am. Chem. Soc.,* 2012, **134**, 6177.

16   M. L. Chabinyc, M. F. Toney, R. J. Kline, I. McCulloch and M. Heeney, *J. Am. Chem. Soc.,* 2007, **129**, 3226.

17   A. P. Yuen, A.-M. Hor, S. M. Jovanovic, J. S. Preston, R. A. Klenkler, N. M. Bamsey and R. O. Loutfy, *Sol. Energy Mater. Sol. Cells,* 2010, **94**, 2455.

18   G. Wantz, F. Lefevre, M. T. Dang, D. Laliberté, P. L. Brunner and O. J. Dautel, *Sol. Energy Mater. Sol. Cells,* 2008, **92**, 558.

19   F. Liu, S. Ferdous, E. Schaible, A. Hexemer, M. Church, X. Ding, C. Wang and T. P. Russell, *Adv. Mater.,* 2015, **27**, 886.

20   H. C. Liao, C. S. Tsao, T. H. Lin, C. M. Chuang, C. Y. Chen, U. S. Jeng, C. H. Su, Y. F. Chen and W. F. Su, *J. Am. Chem. Soc.,* 2011, **133**, 13064.

21   F. Liu, Y. Gu, C. Wang, W. Zhao, D. Chen, A. L. Briseno and T. P. Russell, *Adv. Mater.,* 2012, **24**, 3947.

22   F. Liu, D. Chen, C. Wang, K. Luo, W. Gu, A. L. Briseno, J. W. Hsu and T. P. Russell, *ACS Appl. Mater. Interfaces,* 2014, **6**, 19876.

23   B. A. Collins, J. E. Cochran, H. Yan, E. Gann, C. Hub, R. Fink, C. Wang, T.

Schuettfort, C. R. McNeill, M. L. Chabinyc and H. Ade, *Nat. Mater.,* 2012, **11**, 536.

24   F. Liu, C. Wang, J. K. Baral, L. Zhang, J. J. Watkins, A. L. Briseno and T. P. Russell, *J. Am. Chem. Soc.,* 2013, **135**, 19248.

25   M. Xiao, F. Huang, W. Huang, Y. Dkhissi, Y. Zhu, J. Etheridge, A. Gray-Weale, U. Bach, Y. B. Cheng and L. Spiccia, *Angew. Chem.,* 2014, **53**, 9898.

26   K. Chen, Q. Hu, T. Liu, L. Zhao, D. Luo, J. Wu, Y. Zhang, W. Zhang, F. Liu, T. P. Russell, R. Zhu and Q. Gong, *Adv. Mater.,* 2016, **28**, 10718.

27   Z. Xu, L.-M. Chen, G. Yang, C.-H. Huang, J. Hou, Y. Wu, G. Li, C.-S. Hsu and Y. Yang, *Adv. Func. Mater.,* 2009, **19**, 1227.
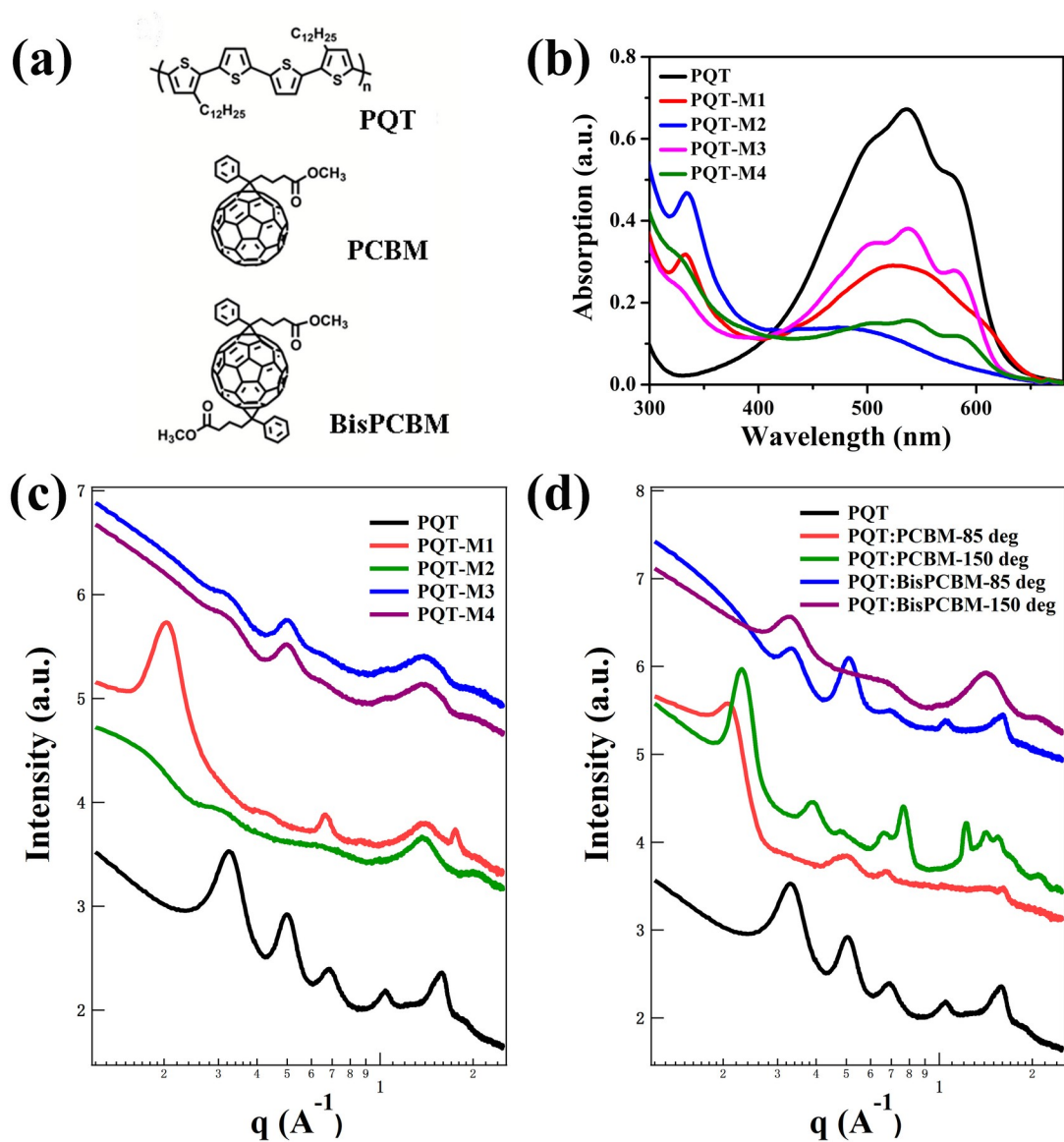
Figures and Figure captions

Fig. 1 (a) Chemical structure of poly(3, 3'''-didodecylquaterthiophene) (PQT). [6, 6]-phenyl C61 butyric acid methyl ester (PCBM), and PCBM bisadduct (BisPCBM). (b) UV-vis absorption spectrum of PQT, PQT-M1, PQT-M2, PQT-M3, and PQT-M4. (c) GIXD profiles of pure PQT, PQT:Fullerene (PCBM or BisPCBM) blends with different weight ratios. (d) GIXD profiles of PQT:Fullerene blends with annealing treatment at different temperatures (85 °C and 150 °C).
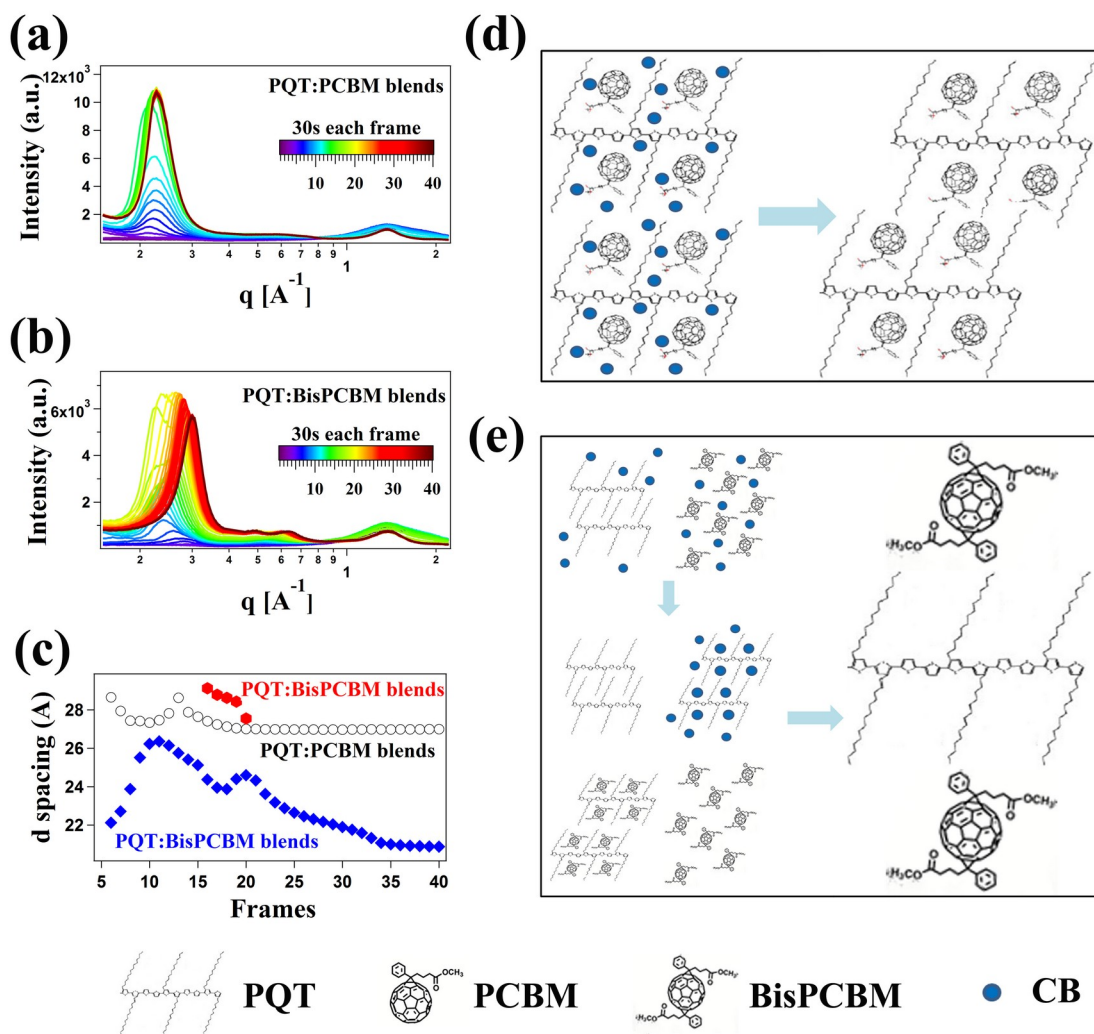
Fig. 2 In-situ integral GIXD profiles of PQT:PCBM (a) and PQT:BisPCBM (b) drying along with time (40 frames). (c) The time (40 frames) evolution of lamellae stacking distance of PQT:Fullerene (PCBM or BisPCBM) blends with the weight ratio of 1:1. (d) and (e) schematic models showing the process of PQT:Fullerene blending films.
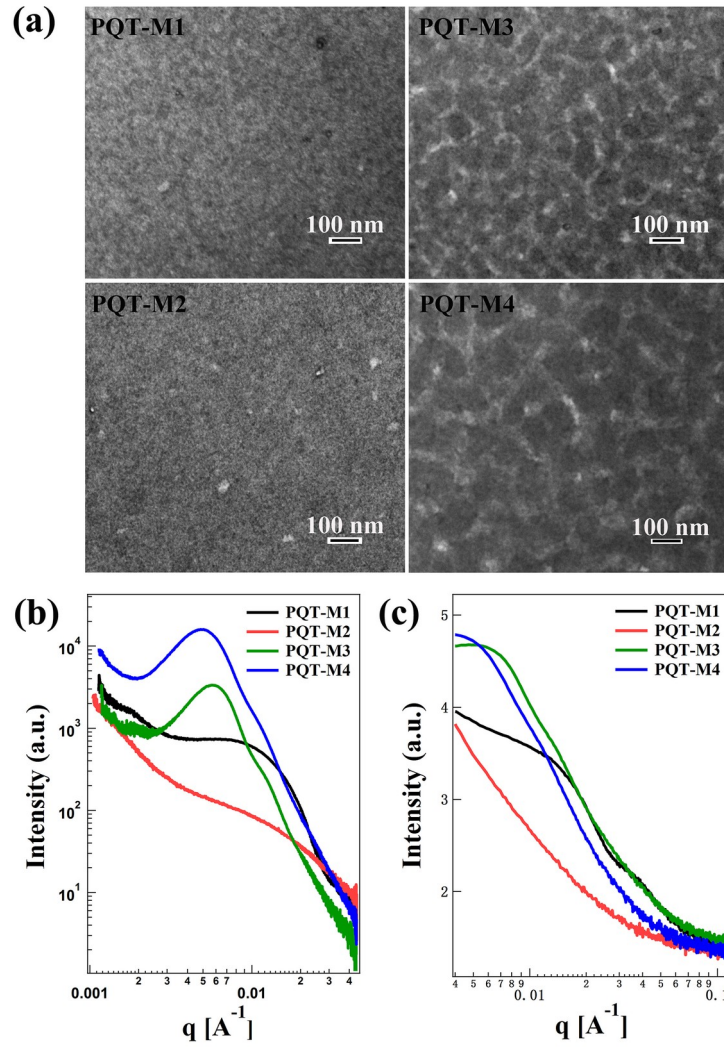
Fig. 3 (a) TEM images (b) Transmission resonant soft X-ray scattering and (C) Grazing incident small angle X-ray scattering (GISAXS) of PQT-M1, PQT-M2, PQT-M3, and PQT-M4.
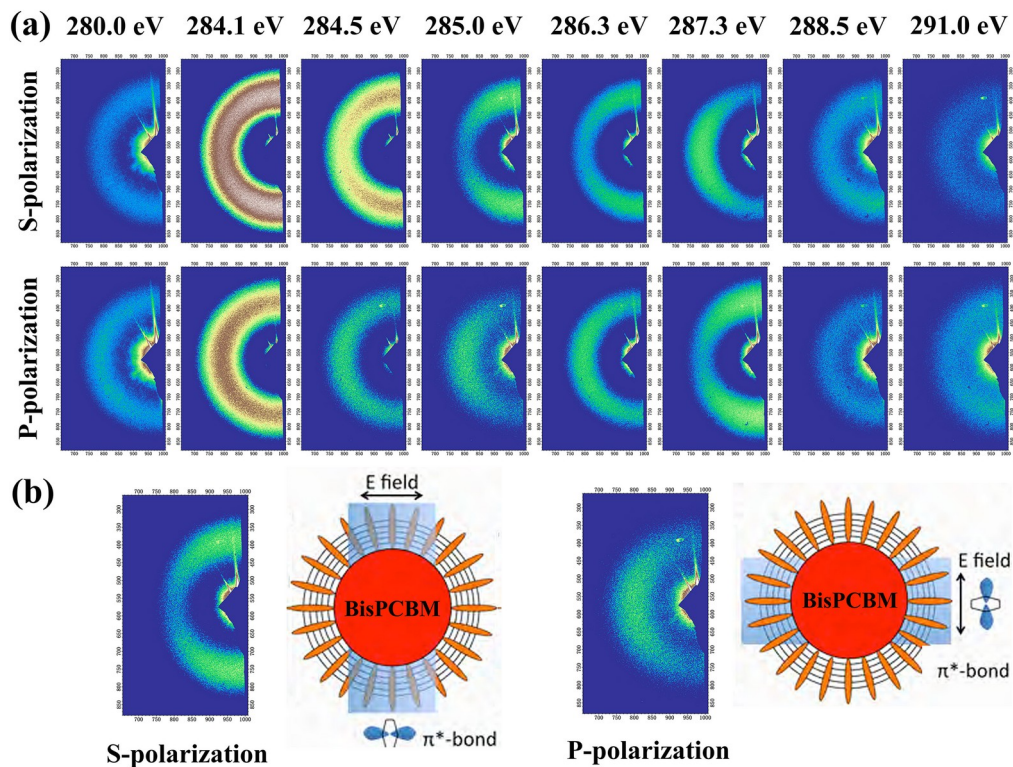
(a) 280.0 eV   284.1 eV   284.5 eV   285.0 eV   286.3 eV   287.3 eV   288.5 eV   291.0 eV

S-polarization

P-polarization

(b)

S-polarization   P-polarization

Fig. 4 (a) Energy and polarization dependent transmission RSoXS images of PQT-M4 blends across the carbon 1s edge, showing the scattering anisotropy near the π^* and σ^* transitions, as well as the local molecular orientation. (b) Polarization dependent scattering patterns from PQT-M4 blends.
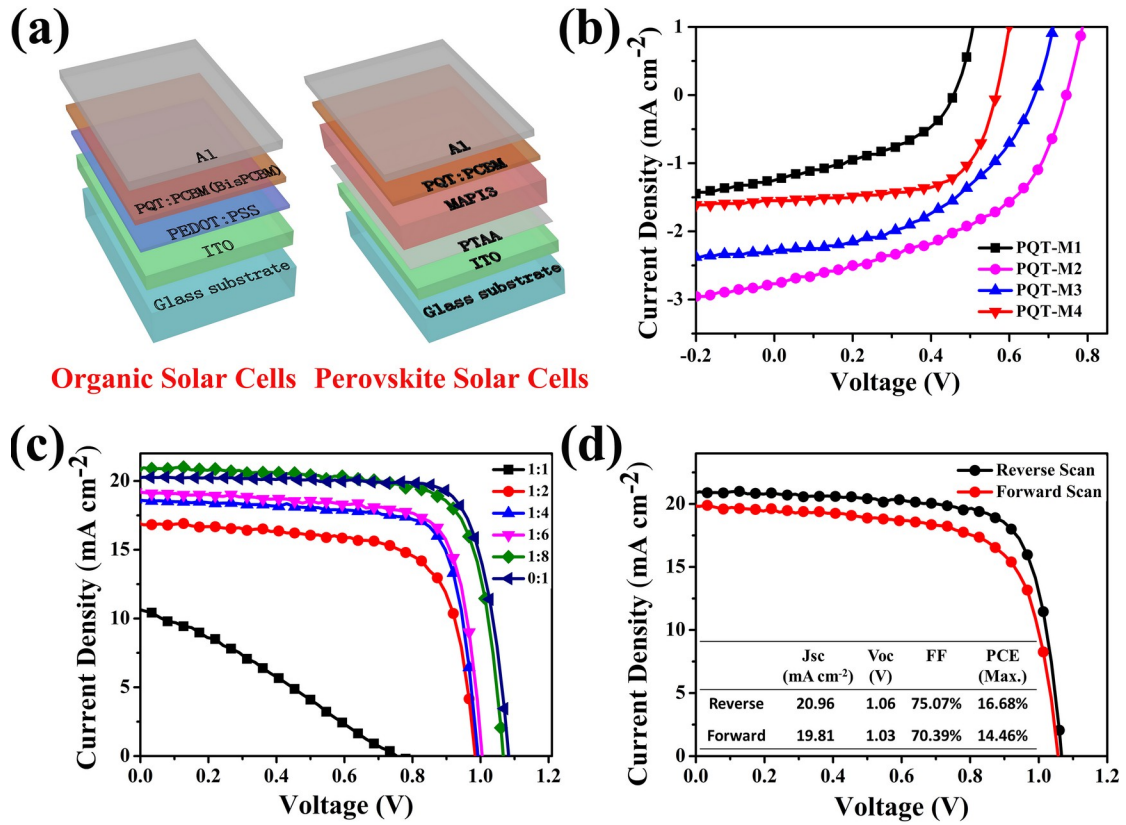
Fig. 5 (a) A schematic representation of the device configuration of bulk-heterojunction (BHJ) organic solar cells and perovskite solar cells. (b) Current density–voltage (J-V) curves of the BHJ solar cells based on different active layers of PQT:PCBM or PQT:BisPCBM. (c) J-V curves of perovskite solar cells with different weight ratios of PQT and PCBM as electron transporting layers. (d) J-V plots of champion perovskite device with the optimal PQT and PCBM weight ratio of 1:8 measured in forward and reverse direction. The inset table shows the detailed device parameters.

TOC Figure
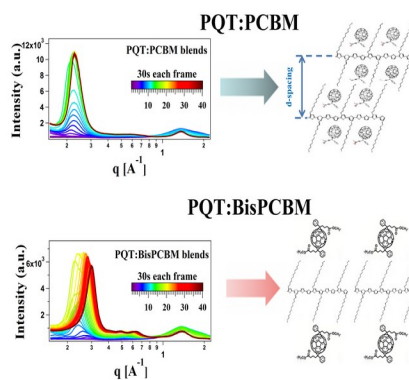
Here, the in-situ GIXD experiments are conducted to investigate the structure evolution process of PQT:Fullerene blends. For the PQT:PCBM blends, the PCBM intercalate into the side chains of PQT, finally forming a stable bimolecular crystals. While for the PQT:BisPCBM blends, BisPCBM is too large to intercalate into the PQT side chains, with the d-spacing similar to that of pure PQT.